Entanglement transitions and quantum bifurcations under continuous long-range monitoring

Angelo Russomanno [1,2] Giulia Piccitto [3,4] and Davide Rossini [3]

[1]*Scuola Superiore Meridionale, Università di Napoli Federico II Largo San Marcellino 10, I-80138 Napoli, Italy*

[2]*Dipartimento di Fisica "E. Pancini", Università di Napoli Federico II, Complesso di Monte S. Angelo, via Cinthia, I-80126 Napoli, Italy*

[3]*Dipartimento di Fisica dell'Università di Pisa and INFN, Largo Pontecorvo 3, I-56127 Pisa, Italy*

[4]*Dipartimento di Matematica e Informatica, Università di Catania, Viale Andrea Doria 6, 95125, Catania, Italy*

(Received 20 July 2023; accepted 7 September 2023; published 18 September 2023)

We study the asymptotic bipartite entanglement entropy of the quantum trajectories of a free-fermionic system, when subject to a continuous nonlocal monitoring. The measurements are described by Gaussian-preserving two-point operators, whose strength decays as a power law with exponent α. Different behaviors of the entanglement entropy with the system size emerge: for α below a given threshold value a volume-law behavior sets in, while for larger α we observe a transition from subvolume to area law, whose exact location depends on the measurements rate and on the presence of a Hamiltonian dynamics. We also consider the expectation probability distribution of the measurement operators, and find that this distribution features a transition from a unimodal to a bimodal shape. We discuss the possible connections between this qualitative change of the distribution and the entanglement transition points.

DOI: 10.1103/PhysRevB.108.104313

I. INTRODUCTION

Nowadays it is widely believed that entanglement, alias a kind of quantum correlations with no classical analog [1,2], plays an important role in the equilibrium and the out-of-equilibrium physics of quantum many-body systems [3]. A prototypical example is that of the entanglement entropy for a pure state, which is defined as the von Neumann entropy of the reduced density matrix of a given portion of the full system. Due to its peculiar scaling properties at the critical point [4,5], it may act as a witness of the presence of quantum phase transitions. Moreover, in nonequilibrium conditions, it generally increases linearly in time to eventually attain an asymptotic value proportional to the system size [6–8], and the slope of this scaling contains information on the thermalization properties of the system [9]. Such scenario changes qualitatively in the presence of disorder: For example, in many-body localized phases, the entanglement entropy undergoes a characteristic, much slower, logarithmic increase in time (see Ref. [10] for a review).

More recently, the focus has been moved to situations beyond the unitary dynamics, which consider the evolution of monitored systems. The interplay between the intrinsic dynamics of the system and that induced by the quantum measurement process can lead to a variety of scaling regimes for the asymptotic entanglement entropy, giving rise to the so called entanglement transitions. In this framework, an extensive number of papers has been focusing on local measurements (either discrete or continuous in time) performed in monitored quantum circuits [11–30], as well as noninteracting [17,31–46] and interacting [47–53] Hamiltonian systems. Moreover, there exists a deep connection between measurement-induced phases and the encoding/decoding properties of a quantum channel [16,54–63]. Situations where the dynamics is only induced by random measurements of nonlocal string operators (measurement-only dynamics) have been also considered, finding different scaling regimes of the entanglement entropy, according to the statistics of the randomly measured operators, and the range and the nature of the strings [64,65].

Among the various theoretical models of monitored quantum systems, considerable coverage has been dedicated to the dynamics of fermionic Gaussian states, in the presence of quadratic Hamiltonians and Gaussian-preserving measurement processes (see, e.g., Refs. [31,34,36,39–46,66–68]), as they are amenable to an accurate numerical treatment up to relatively large sizes. In this framework, for short-range Hamiltonians and local measurements, area-law (saturation to a finite value) or logarithmic scaling of the asymptotic entanglement entropy with the system size have been reported. A somewhat richer situation has been found for Hamiltonians with extended power-law interactions, although keeping the measurement operators on-site, where regimes with a power-law scaling of the entanglement entropy with the system size are possible [67,69]. Something similar has been considered in the context of quantum circuits [70,71]. In a recent paper, we have also shown that the measurement-only dynamics through operators connecting two distant sites can give rise to a nontrivial entanglement entropy dynamics, with a fast growth with the system size of the asymptotic entanglement entropy [72].

In this paper we deal with the quantum dynamics of a Kitaev chain under continuous nonlocal monitoring, which can be cast as a quantum state diffusion unraveling [73,74] of a Lindblad master equation with long-range Lindblad operators. Specifically, we consider two-point fermionic measurement operators, suitably chosen to preserve Gaussianity, where the coupling decays as a power law with some exponent $\alpha > 0$. In the context of dissipation engineering, similar kind of dissipators have been already scrutinized in some recent papers [75–78]; these can be realized with two-level atoms in lossy cavity QED experiments, using a magnetic field gradient

and a Raman drive with multiple sidebands [75]. In noninteracting spins monitored by infinite-range operators, an entanglement transition from area-law to sublogarithm scaling can occur [79].

Here we first consider the asymptotic bipartite entanglement entropy and find a rather rich phenomenology: For α smaller than a threshold value $\alpha_1^\star$, it obeys a volume law, suggesting a strong entangling power of the long-range measurement operators. For intermediate values of α, a crossover region emerges, in which the entanglement entropy scales nontrivially with the size. For α larger than $\alpha_2^\star$ ($> \alpha_1^\star$), we recover the area-law scaling observed in the presence of on-site measurements. The fact that $0.5 \lesssim \alpha_1^* \lesssim 1$, independently of the Hamiltonian parameters and of the coupling with the measurement apparatus, is suggestive. Indeed, $\alpha = 1$ corresponds to the threshold below which both the unitary (Hamiltonian) long-range dynamics in one dimension [80,81] and at least a single case of Lindblad long-range dynamics in one dimension [78] are exactly described by the mean-field approximation.

We also focus on a measurement-only dynamics, i.e., such that there is no Hamiltonian providing a unitary part in the evolution. In that case, we still have evidence that $0.5 \lesssim \alpha_1^* \lesssim 1$. Besides that we can locate the transition point between subvolume and area-law behavior at $\alpha_2^* \sim 2$, suggesting an even more interesting comparison with the behavior of long-range Hamiltonians, where the system behaves short range above the threshold $\alpha = 2$ [80,81].

Finally, we study the expectation probability distribution of the measurement operators. When increasing α, the distribution over a single quantum trajectory of the expectation values of such operators undergoes a transition from unimodal (one maximum) to bimodal (two maxima), at a point $\bar{\alpha}$ that is not immediately related with the change of scaling for the entanglement entropy. Such transition is reminiscent of the bifurcations occurring in nonlinear-driven dissipative classical dynamical systems, where a single stable stationary point splits into two [82,83]. Here, due to the presence of quantum fluctuations and classical noise, there are no stationary points, and their equivalent are the maxima of the distribution that move from being one to two. In view of this analogy, we dub the unimodal-bimodal transition of the distribution of the expectations as a "quantum bifurcation".

The paper is organized as follows. In Sec. II, we define our model, specifying both the Hamiltonian and the measurement operators, together with the bipartite entanglement entropy we are going to analyze. In Sec. III, we introduce the quantum state diffusion unraveling of the Lindblad master equation and discuss how to treat the time evolution of the system, preserving the Gaussian form of the wavefunction. Section IV is devoted to the presentation of our numerical findings summarized above, for the entanglement entropy (Sec. IV A) and for the expectation distribution of the measurement operators (Sec. IV B). In Sec. V we draw our conclusions.

II. MODEL

We start from a system of spinless fermions on a one-dimensional lattice with N sites, described by the Kitaev Hamiltonian [84]

$$\hat{H} = \sum_i [J(\hat{c}_i - \hat{c}_i^\dagger)(\hat{c}_{i+1} + \hat{c}_{i+1}^\dagger) + 2h\,\hat{c}_i^\dagger \hat{c}_i]. \tag{1}$$

The real constants J and h stand for, respectively, the nearest-neighbor coupling and the chemical potential $\mu \equiv 2h$, while $\hat{c}_i^{(\dagger)}$ are annihilation (creation) operators on the ith site ($i = 1, \ldots, N$), exhibiting canonical anticommutation relations. The Hamiltonian (1) is responsible for the unitary part of the dynamics. We notice that this model can be mapped, via a Jordan-Wigner transformation, onto a quantum Ising chain in a transverse field [85,86]. Hereafter, we set $J = 1$ as a energy scale and work in units of $\hbar = 1$.

We consider the Lindblad master equation

$$\frac{d}{dt}\rho(t) = -i[\hat{H}, \rho(t)] + \frac{\gamma}{2}\sum_i (\{\hat{\ell}_i^\dagger \hat{\ell}_i, \rho\} - 2\,\hat{\ell}_i \rho\, \hat{\ell}_i^\dagger) \tag{2}$$

with measurement operators

$$\hat{\ell}_i = \sum_j f_{ij}(\hat{c}_i - \hat{c}_i^\dagger)(\hat{c}_j + \hat{c}_j^\dagger), \tag{3}$$

and focus on its quantum state diffusion unraveling. This corresponds to a continuous time monitoring of the system, which is described by the following stochastic Schrödinger equation for the pure state $|\psi_t\rangle$:

$$\begin{aligned} d|\psi_t\rangle = &-i\hat{H}dt\,|\psi_t\rangle + \sum_i \Big(\sqrt{\gamma}[\hat{\ell}_i - \langle\hat{\ell}_i\rangle_t]dW_t^i \\ &- \frac{\gamma}{2}[\hat{\ell}_i - \langle\hat{\ell}_i\rangle_t]^2 dt\Big)|\psi_t\rangle\,, \end{aligned} \tag{4}$$

where $\gamma > 0$ is the coupling strength with the measurement apparatus, $\langle\hat{\ell}_i\rangle_t = \langle\psi_t|\,\hat{\ell}_i\,|\psi_t\rangle$, and W_t^i are independent Wiener processes describing a quantum state diffusion process that unravel the equation (2).

In Eq. (3), the real prefactor f_{ij} is assumed to algebraically decay with the distance $D_{i,j}$ between site i and site j, such that

$$f_{ij} = \frac{1}{N(\alpha)}\frac{1}{(1 + D_{i,j})^\alpha}, \qquad (\alpha \geqslant 0). \tag{5}$$

Here $N(\alpha) = (N-1)^{-1}\sum_{i,j}(1 + D_{i,j})^{-\alpha}$ is a proper normalization constant (the Kac factor), ensuring extensivity in the system [87]. In what follows, we choose periodic boundary conditions for fermions (such that $\hat{c}_{j+N}^{(\dagger)} \equiv \hat{c}_j^{(\dagger)}$, for any $j > N$), consequently $D_{i,j} = \min(|i-j|, N - |i-j|)$. Notice also that the $\hat{\ell}_i$ are Hermitian, $\hat{\ell}_i = \hat{\ell}_i^\dagger$.

An important property of the operators $\hat{\ell}_i$ is that

$$\hat{\ell}_i^2 = \sum_{j,l} f_{ij} f_{il}(\hat{c}_j + \hat{c}_j^\dagger)(\hat{c}_l + \hat{c}_l^\dagger) = \sum_j f_{ij}^2, \tag{6}$$

where we used the anticommutation relations for fermions and the fact that $(\hat{c}_i - \hat{c}_i^\dagger)^2 = -1$. Thanks to this property, Eq. (4) can be seen as a Schrödinger equation with a non-Hermitian quadratic Hamiltonian. As a consequence, the state $|\psi_t\rangle$ keeps a simple Gaussian form, described by just $N(N-1)/2$ complex independent parameters, as we better discuss in Sec. III. One can thus push the numerics to system sizes of some hundreds of sites and investigate how the presence of power-law decaying measurement operators affects the production of entanglement during the quantum dynamics.

To this purpose, we concentrate on the entanglement entropy of a subchain of length l, averaged over different quantum trajectories

$$\overline{S_l(t)} \equiv -\overline{\mathrm{Tr}[\rho_l \ln \rho_l]}, \tag{7}$$

where the logarithm is taken in the natural basis. Here, $\rho_l(t) = \mathrm{Tr}_{N-l}[|\psi_t\rangle\langle\psi_t|]$ is the reduced density matrix of the subchain and $|\psi_t\rangle$ is the (pure) state of a single quantum trajectory given by a single realization of the stochastic Schrödinger equation dynamics in Eq. (4) (see also Sec. III).

To obtain the average entanglement entropy, we evaluate it on each single stochastic quantum trajectory and then ensemble-average over different realizations. In our analysis, we will mostly focus on the asymptotic long-time value

$$S_l = \lim_{T\to\infty} \int_{t^*}^{T} dt' \, \overline{S_l(t')}. \tag{8}$$

As discussed in Ref. [88], for fermionic Gaussian states, the entanglement entropy can be determined from the knowledge of the correlation functions, that are introduced in the next section.

III. DYNAMICS UNDER CONTINUOUS MONITORING

Equation (4) can be discretized in time and cast as a sequence of Trotterized evolution steps that in the limit $\Delta t \to 0$, converge back to Eq. (4) [31]. In each Trotterized step, the measurement and the unitary part of the dynamics act separately and in sequence,

$$|\psi_{t+\Delta t}\rangle \simeq C\, \mathrm{e}^{\sum_i (A_i \hat{\ell}_i - \gamma \hat{\ell}_i^2 \Delta t)}\, \mathrm{e}^{-i\hat{H}\Delta t}\, |\psi_t\rangle\,, \tag{9}$$

where we have defined

$$A_i \equiv \sqrt{\gamma}\, \Delta W_t^i + 2\gamma\, \langle \hat{\ell}_i \rangle_t\, \Delta t, \tag{10}$$

with ΔW_t^i being independent real Gaussian random variables with vanishing expectation value and variance Δt.

Expression (9) can be further simplified by using Eq. (6). In this way one can rewrite Eq. (9) in the simpler form

$$|\psi_{t+\Delta t}\rangle \simeq \tilde{C}\, \mathrm{e}^{\sum_i A_i \hat{\ell}_i}\, \mathrm{e}^{-i\hat{H}\Delta t}\, |\psi_t\rangle\,, \tag{11}$$

where the irrelevant constant $\exp(-\gamma\, \Delta t \sum_j f_{ij}^2)$, coming from the exponential of $\hat{\ell}_i^2$, has been absorbed into the normalization prefactor $\tilde{C}$.

Being both $\hat{\ell}_i$ and the Kitaev Hamiltonian quadratic in the fermionic operators $\hat{c}_j^{(\dagger)}$, when starting from an initial Gaussian state, the time evolution of Eq. (11) preserves Gaussianity. In particular, the state $|\psi_t\rangle$ can be cast as

$$|\psi_t\rangle = \mathcal{N}_t\, \exp\left(\frac{1}{2}\sum_{j_1,j_2} [\mathbf{Z}_t]_{j_1,j_2} \hat{c}_{j_1}^\dagger \hat{c}_{j_2}^\dagger\right) |0\rangle, \tag{12}$$

where $|0\rangle$ denotes the vacuum state of the $\hat{c}$ fermions, and is thus uniquely described by the $N \times N$ antisymmetric matrix $\mathbf{Z}_t$ [being $\mathbf{Z}_t$ antisymmetric, it is described by $N(N-1)/2$ complex parameters]. From the matrix $\mathbf{Z}_t$, one can easily derive any two-point correlation functions. Defining

$$[\mathbf{G}_t]_{j,l} \equiv \langle\psi_t|\hat{c}_l^\dagger \hat{c}_j|\psi_t\rangle\,, \quad [\mathbf{F}_t]_{j,l} \equiv \langle\psi_t|\hat{c}_l\, \hat{c}_j|\psi_t\rangle\,, \tag{13}$$

the correlation matrices can be written in terms of the matrix $\mathbf{Z}_t$ as [89]

$$\mathbf{G}_t = (\mathbf{1} + \mathbf{Z}_t\, \mathbf{Z}_t^\dagger)^{-1} \mathbf{Z}_t\, \mathbf{Z}_t^\dagger, \quad \mathbf{F}_t = (\mathbf{1} + \mathbf{Z}_t\, \mathbf{Z}_t^\dagger)^{-1} \mathbf{Z}_t, \tag{14}$$

where $\mathbf{1}$ is the $N \times N$ identity matrix. Being $\mathbf{Z}_t^T = -\mathbf{Z}_t$, we see that $\mathbf{G}_t = \mathbf{G}_t^T$ and $\mathbf{F}_t = -\mathbf{F}_t^T$.

In the next subsection we show a simple numerical prescription (whose computational requirements scale polynomially with N) to evaluate the matrix $\mathbf{Z}_t$ after the application of the unitary and the dissipative part of the evolution step in Eq. (11) (and, therefore, the entanglement entropy).

Evolution of the matrix $\mathbf{Z}_t$

It is possible to write a system of ordinary differential equations for the matrix $\mathbf{Z}_t$, describing the evolution in Eq. (12) and efficiently solvable (an alternative derivation can be found in Ref. [72]).

Both the action of the unitary step and the measurement step in Eq. (11) can be described as the application, to a Gaussian state of the form Eq. (12), of an operator of the form $\mathrm{e}^{-\xi \hat{T}\Delta}$, where

$$\hat{T} = \sum_{i,j} (\mathbf{D}_{i,j}\, \hat{c}_i^\dagger \hat{c}_j + \mathbf{O}_{i,j}\, \hat{c}_i^\dagger \hat{c}_j^\dagger + \mathrm{H.c.}) \tag{15}$$

is a generic (Hermitian) quadratic operator, Δ is real, and $\xi = \{i, -1\}$ accounts for a dynamics in real or in imaginary time, respectively. Let us define $|\psi\rangle$ as a Gaussian state of the form (12), to which we apply the operator $\mathrm{e}^{-\xi \hat{T}\Delta}$, and $\mathbf{Z}$ the corresponding antisymmetric matrix. After this operation the state $|\psi'\rangle \equiv \mathrm{e}^{-\xi \hat{T}\Delta}|\psi\rangle$ [being $|\psi\rangle$ a generic Gaussian state described by the matrix $\mathbf{Z}$, as in Eq. (12)] is still Gaussian, and its corresponding $\mathbf{Z}'$ matrix is obtained by integrating the system of ordinary differential equations

$$\xi \frac{d}{ds}\mathbf{Z}(s) = 2[\mathbf{D}\cdot\mathbf{Z}(s) + \mathbf{Z}(s)\cdot\mathbf{D} + \mathbf{O} + \mathbf{Z}(s)\cdot\mathbf{O}\cdot\mathbf{Z}(s)], \tag{16}$$

from $s = 0$ to Δ, with initial conditions $\mathbf{Z}(0) \equiv \mathbf{Z}$, as shown in Ref. [89].

The unitary step of Eq. (11) is obtained by posing $\xi = i$, $\Delta = \Delta t$, and $\hat{T} = \hat{H}$, such that

$$\begin{aligned} &\mathbf{D}_{i,i+1} = \mathbf{D}_{i,i-1} = -J/2, \quad \mathbf{D}_{i,i} = h, \\ &\mathbf{O}_{i,i+1} = -\mathbf{O}_{i,i-1} = -J/2, \end{aligned} \tag{17}$$

and zero otherwise. Analogously, the dissipative step can be obtained by posing $\xi = -1$, $\Delta = 1$, and $\hat{T} = \sum_i A_i \hat{\ell}_i$ [A_i are the real coefficients defined in Eq. (10)]. Using the anticommutation relations and the symmetry of the couplings $f_{ij} = f_{ji}$, we can write

$$\begin{aligned} \sum_i A_i \hat{\ell}_i &= \sum_{i,j} [A_i f_{ij} (\hat{c}_i \hat{c}_j + \hat{c}_j^\dagger \hat{c}_i) + \mathrm{H.c.}] \\ &= \frac{1}{2}\sum_{i,j} [(A_i - A_j) f_{ij} \hat{c}_i \hat{c}_j + (A_i + A_j) \hat{c}_j^\dagger \hat{c}_i + \mathrm{H.c.}], \end{aligned} \tag{18}$$

so that in Eq. (16) one has

$$\mathbf{D}_{i,j} = -\frac{1}{2}(A_i + A_j) f_{ij} \quad \mathbf{O}_{i,j} = -\frac{1}{2}(A_i - A_j) f_{ij}. \tag{19}$$

Defining $N \times N$ matrices $\mathbf{U}(s)$, $\mathbf{V}(s)$ such that

$$\mathbf{U}^\dagger(s)\,\mathbf{Z}(s) = -\mathbf{V}^\dagger(s), \tag{20}$$

we can show [90] that, if and only if $\mathbf{Z}(s)$ obeys Eq. (16), then $\mathbf{U}(s)$ and $\mathbf{V}(s)$ satisfy the linear system of differential equations

$$\xi \frac{d}{ds}\begin{pmatrix}\mathbf{U}(s)\\ \mathbf{V}(s)\end{pmatrix} = \begin{pmatrix}\mathbf{D} & \mathbf{O}\\ -\mathbf{O} & -\mathbf{D}\end{pmatrix}\begin{pmatrix}\mathbf{U}(s)\\ \mathbf{V}(s)\end{pmatrix}. \tag{21}$$

This can be straightforwardly integrated to give [72,88]

$$\begin{pmatrix}\mathbf{U}'\\ \mathbf{V}'\end{pmatrix} = \exp\left[-2\xi\Delta\begin{pmatrix}\mathbf{D} & \mathbf{O}\\ -\mathbf{O} & -\mathbf{D}\end{pmatrix}\right]\begin{pmatrix}\mathbf{U}(0)\\ \mathbf{V}(0)\end{pmatrix}, \tag{22}$$

where $\mathbf{U}(0)$ and $\mathbf{V}(0)$ correspond to the initial condition $\mathbf{Z}(0)$ for $|\psi\rangle$.

The above observation provides a direct and simple solution to the problem of finding how the matrix $\mathbf{Z}$ of a Gaussian state, as that in Eq. (12), is modified after the evolution (11). The latter is composed of a unitary step, followed by a dissipative step: Any time a given operator of the form $e^{-\xi\hat{T}\Delta}$ is applied to the state (12), the matrix $\mathbf{Z} \equiv -[\mathbf{U}^\dagger]^{-1}\,\mathbf{V}^\dagger$ is transformed into $\mathbf{Z}' \equiv -[\mathbf{U}'^\dagger]^{-1}\,\mathbf{V}'^\dagger$, the matrices $\mathbf{U}'$ and $\mathbf{V}'$ being expressed as in Eq. (22).

In the measurement step, to restore the normalization of the state it is necessary to perform the QR decomposition

$$\begin{pmatrix}\mathbf{U}'\\ \mathbf{V}'\end{pmatrix} = \begin{pmatrix}\mathbf{U_Q}\\ \mathbf{V_Q}\end{pmatrix}\mathbf{R}, \tag{23}$$

where $\mathbf{R}$ is a $L \times L$ upper triangular matrix and $\mathbf{U_Q}$ and $\mathbf{V}_Q$ obey the unitarity condition $\mathbf{U}_Q^\dagger\mathbf{U}_Q + \mathbf{V}_Q^\dagger\mathbf{V}_Q = \mathbf{1}$. From the one side, the QR decomposition does not modify the matrix $\mathbf{Z}$ that defines the state, since it is easy to check that $\mathbf{Z}' = -[\mathbf{U}'^\dagger]^{-1}\,\mathbf{V}'^\dagger = -[\mathbf{U}_Q^\dagger]^{-1}\,\mathbf{V}_Q^\dagger$. From the other side, it restores unitarity [31,72], allowing the evaluation of the correlation matrices as

$$\mathbf{G}' = \mathbf{1} - \mathbf{U}_Q\mathbf{U}_Q^\dagger, \quad \mathbf{F}' = -\mathbf{U}_Q\mathbf{V}_Q^\dagger, \tag{24}$$

as one can easily check by substituting $\mathbf{Z}' = -[\mathbf{U}_Q^\dagger]^{-1}\,\mathbf{V}_Q^\dagger$ in Eqs. (14) and by imposing the unitarity condition.

IV. RESULTS

The results presented below have been obtained by initializing the system in the ground state of the Hamiltonian Eq. (1) with $J = 1$, $h_i = 100$, and letting it evolve under continuous monitoring after a sudden quench of the field to $h = 0.5$. We checked that the asymptotic value of the entanglement entropy, as well as the expectation probability distribution of the measurement operators, are not affected by the choice of h_i and weakly depend on h. Therefore, without loss of generality, hereafter we keep them fixed.

To compute the entanglement entropy, we choose a balanced bipartition by taking $l = N/2$ [see Eq. (7)], and finally perform the averages in Eqs. (7) and (8) over a given number N_r of realizations of the stochastic process. On the other hand, to obtain the expectation probability distribution of the measurement operators, we evolve a single quantum trajectory up to a long time $\mathcal{T}$. Details on the convergence of our numerical results are provided in Appendix A.

A. Entanglement entropy

1. Dynamics with unitary and measurement parts

We specifically address the behavior of the average asymptotic entanglement entropy [see Eq. (8)] as a function of the system size N and of the power-law exponent α for the measurement operator. We first consider a free-fermionic system described by the Kitaev Hamiltonian Eq. (1), and continuously monitored through the long-range operators Eq. (3).

In Fig. 1(a) we show $S_{N/2}$ versus the system size N, for different values of α (color gradient). We notice that, for $\alpha \lesssim 1$, it exhibits a volume-law scaling (i.e., it grows linearly with N). When increasing the power-law exponent, the curves bend to eventually show a flat profile, for very large α. This behavior suggest the emergence of a volume-law behavior in the long-range regime ($\alpha < 1$) that, after a crossover for intermediate values of α, turns into an area-law behavior at short-range monitoring ($\alpha \gg 1$).

This can be appreciated more clearly in Fig. 1(b), where we plot the normalized asymptotic entanglement $S_{N/2}/N$ versus the power-law exponent α. As expected, for $\alpha \lesssim 1$ the curves for different values of N collapse to a finite value, evidencing a linear scaling with N. On the other hand, for $\alpha \gtrsim 3.5$, the curves approach the zero value, thus signaling the onset of a regime where the dependence of S_l with N is very weak, if not absent (meaning area-law behavior). In the intermediate regime $1 \lesssim \alpha \lesssim 3.5$, we also observe a less-than-linear dependence on the system size, which is more difficult to characterize properly.

Further insight on the sublinear region ($\alpha \gtrsim 1$) can be obtained after rescaling the entropy by $\ln(N)$, as in Fig. 1(c). In particular, looking at the inset, the curves for different system sizes exhibit a crossing at $\alpha \sim 3.2$. This should correspond to a value marking the transition between a more-than-logarithmic and a sublogarithmic (most probably area-law) dependence with N. At this point we should note that, since for $\alpha > 2$ the measurement operators have a short-range character, one cannot rule out the possibility to have a further transition in the intermediate region, from a power law (sublinear) to a logarithmic scaling, before ending up into an area-law region at $\alpha \gtrsim 3.2$. Although hardly visible from our numerical data, the possible occurrence of a logarithmic scaling could be of the same kind of those emerging in free-fermionic systems in the presence of local monitoring [32,36,39,41].

Summarizing, we can locate two special points $\alpha_1^\star$ and $\alpha_2^\star$ separating three regions with qualitatively different behaviors in the entropy scaling with N (increasing α, we have volume-law, intermediate subvolume, and area-law scalings of S_l with N). To the best of our numerics, for $\gamma = 0.1$ (corresponding to the data reported in Fig. 1), the turning points correspond to $0.5 \lesssim \alpha_1^\star \lesssim 1$ and $\alpha_2^\star \sim 3.2$. While the position of $\alpha_1^\star$ is quite robust when changing the Hamiltonian parameters, this seems not to be the case for $\alpha_2^\star$. In fact, we have performed simulations for other values of γ (see, e.g., the data for $\gamma = 0.5$ in Appendix B) and found that, while the three above

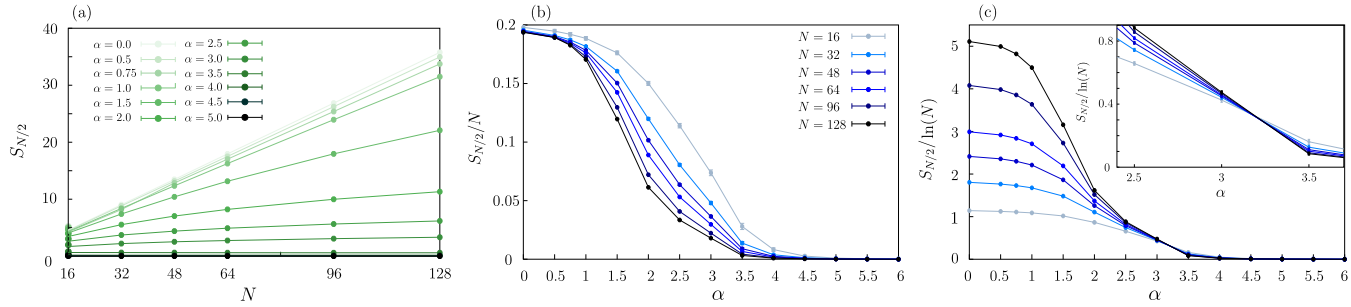

FIG. 1. Behavior of the average long-time entanglement entropy $S_{N/2}$ for a system of free fermions, governed by the interplay between the Kitaev-Hamiltonian dynamics and the long-range monitoring. (a) The entanglement entropy $S_{N/2}$ vs N, for different values of α (increasing α corresponds to a darker color code, as indicated in the legend). (b) $S_{N/2}$ divided by N vs α, for different sizes (increasing N corresponds to darker markers). (c) $S_{N/2}$ divided by $\ln N$ vs α, for different sizes [same sizes and markers as in panel (b)]. The inset is a magnification of the same data around $\alpha = 3$. We fix $\gamma = 0.1$, $J = 1$, and h: $100 \to 0.5$. Numerical parameters: $\Delta t = 5 \times 10^{-3}$, $N_r \geqslant 48$, errorbars as in Appendix A.

regimes (volume law, intermediate crossover, and area law) are still present, the transition point from the intermediate to the area-law behavior moves to different values of the power-law exponent (namely, $\alpha_2^\star$ decreases with increasing γ). On the opposite hand, we always find $0.5 \lesssim \alpha_1^\star \lesssim 1$.

2. *Measurement-only dynamics*

We now switch to the study of a measurement-only dynamics, i.e., for the case without a Hamiltonian providing a unitary part in the dynamics ($J = h = 0$). The plot of $S_{N/2}/N$ versus α is provided in Fig. 2(a) [corresponding to Fig. 1(b) for the case with Hamiltonian], and $S_{N/2}/\ln N$ versus α can be found in Fig. 2(b) [corresponding to Fig. 1(c) for the case with Hamiltonian].

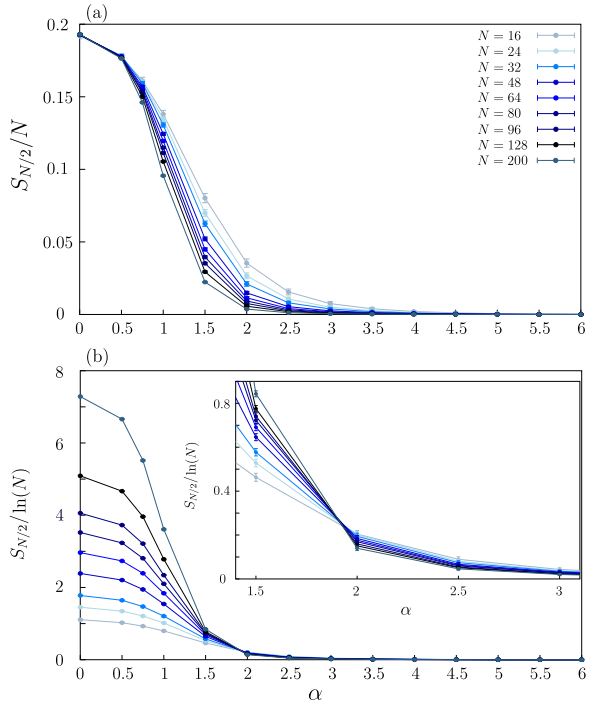

FIG. 2. Average long-time entanglement entropy for the case of measuring-only dynamics (no Hamiltonian, $J = h = 0$). (a) $S_{N/2}/N$ vs α for different system sizes. (b) $S_{N/2}/\ln N$ versus α for different system sizes. The inset is a magnification of the same data around $\alpha = 2$. Numerical parameters: $\gamma \Delta t = 5 \cdot 10^{-4}$, $N_r \geqslant 48$, errorbars as in Appendix A, same initial state as in Fig. 1.

We notice that the behavior in the small α dynamics is quite stable and, in particular, it exhibits a volume-law scaling with L, for $\alpha \lesssim 1$. This suggests that the transition point at $0.5 \lesssim \alpha_1^\star \lesssim 1$ should not depend on the presence of a Hamiltonian and that it is a property of the measurement operators only. There is still an intermediate region featuring a subvolume scaling that vanishes at $\alpha_2^\star \sim 1.9$, corresponding to the intersection point of the curves $S_{N/2}/\ln N$ [c.f., the crossing point for the curves in the inset of Fig. 2(b)].

The fact that α_1^* appears to be independent of the system parameters suggests us a comparison with other long-range systems. From one side, it is known that long-range Hermitian Hamiltonians in one dimension behave mean field for $N \to \infty$ for $\alpha < 1$, short range for $\alpha > 2$, and for $1 < \alpha < 2$ there is an intermediate regime where the excited states of the system can break a symmetry, but in a non-mean-field way [80,81]. In the case without Hamiltonian, the dynamics is provided by a long-range noisy (pseudo) Hamiltonian in imaginary time [see Eq. (4)], and it is interesting that the transition points of the dynamics ($0.5 \lesssim \alpha_1^* \lesssim 1$ and $\alpha_2^* \sim 1.9$) approximately coincide with those of the unitary dynamics. We also recall that, at least in one case [78], $\alpha = 1$ is the threshold below which a mean-field description is exact for $N \to \infty$ in a Lindblad dynamics in one dimension with long-range Lindbladians.

We conclude the section with a remark on the behavior of α_2^*. Considering that the measurement-only case corresponds to the limit of infinite γ (more precisely $\gamma \gg h, J$), we find that α_2^* decreases with γ, as we can see in Table I.

TABLE I. Values of α_2^* vs γ. ($h = 0.5$, $J = 1$ for the first two rows). More details on the case $\gamma = 0.5$ in Appendix B.

γ	α_2^*
0.1	∼3.5
0.5	∼2.4
∞ (measurement only)	∼1.9

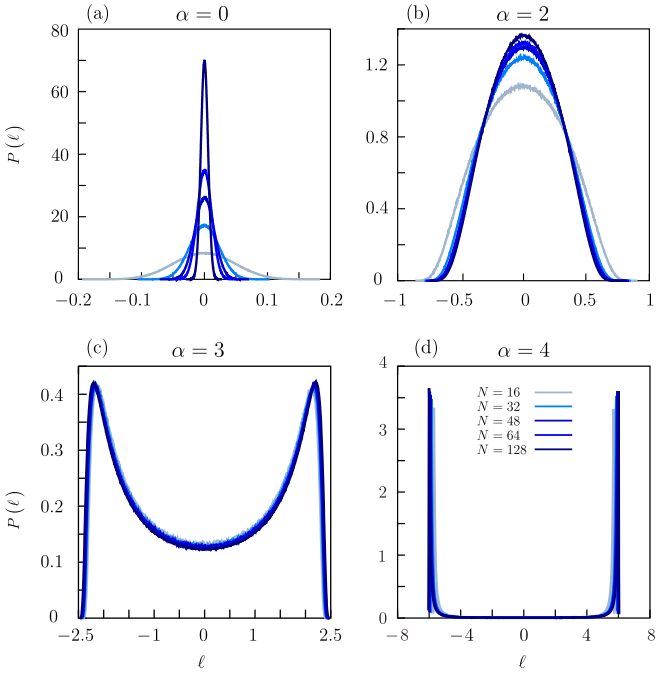

FIG. 3. Probability distributions of the expectations ℓ of measurement operators, over the sites (j) and the discretized time (t), for various system sizes (see legend), The four panels correspond to different values of $\alpha = 0, 2, 3, 4$. Here we fix $\gamma = 0.1$, $J = 1$, and $h : 100 \to 0.5$. Averages over one single quantum trajectory, evolution up to $\mathcal{T} = 10^4$, other numerical parameters as in Fig. 1.

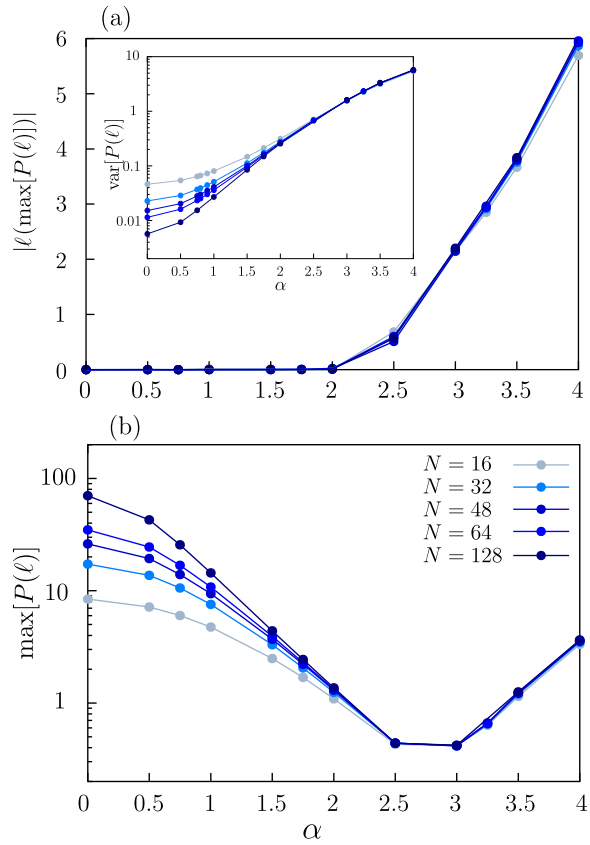

FIG. 4. (a) Absolute value of the position of the maximum of the distributions of the ℓ versus α, for different values of N. The inset shows the variance of the distribution vs α, for different sizes. (b) Absolute maximum of the distribution vs α for different sizes. Same parameters as in Fig. 3.

B. Expectation probability distribution of the measurement operators

We now consider the statistics of the expectations of the measurement operators, a quantity that is experimentally more relevant, being provided by the expectation values of a physically observable operator. Recent studies have pointed out that, for local measurements, the different properties of this distribution or related quantities may be connected to the entanglement transitions [45,91,92].

Operatively, we consider a single quantum trajectory, evolve it up to a time $\mathcal{T}$ with a given discretization time Δt, and evaluate all the expectations $\langle \hat{\ell}_j \rangle_{t_n}$, for the different discrete times $t_n = n\,\Delta t$, $(n = 1, \ldots, \mathcal{T}/\Delta t)$, and the different sites $j = 1, \ldots, N$. Then we arrange these data into a normalized histogram. This is the distribution of the expectations of the measurement operators and we call it $P(\ell)$.

In Fig. 3 we show, for the dynamics of the monitored Kitaev chain with $\gamma = 0.1$, the histograms of the probability of ℓ for $\alpha = 0$ (a), $\alpha = 2$ (b), $\alpha = 3$ (c), and $\alpha = 4$ (d). The various curves in each panel are for different system sizes (color gradient—see legend). The distributions for $\alpha > 1$ tend to a limit for increasing system size, while for $\alpha \leqslant 1$ there is a rescaling (i.e., in the latter case, the distributions converge to a limit, if appropriately rescaled).

It is evident that the shape of such distribution exhibits a crossover from a unimodal to a bimodal character, depending on the value of α. As we have already emphasized, this is reminiscent of bifurcations in nonlinear classical driven-dissipative dynamical systems [82,83], where one stationary point splits into two. Here we have also quantum fluctuations and classical noise, so instead of having stationary points, we have maxima that move to be one (unimodal) to be two (bimodal).

To locate the turning point $\bar{\alpha}$, in the main panel of Fig. 4(a) we plot the absolute value of the position of the maximum $|\ell(\max[P(\ell)])|$ versus α. The latter starts deviating from zero at $\bar{\alpha} \gtrsim 2$, that is far from both the crossover points we identified from the entanglement dynamics ($0.5 \lesssim \alpha_1^\star \lesssim 1$ and $\alpha_2^\star \sim 3.2$, for $\gamma = 0.1$). The inset of Fig. 4(a) shows the variance of the distribution (logarithmic scale on the y-axis). For $\alpha \lesssim 1$ the variance is size dependent, meaning that the distribution shrinks when increasing N. This dependence is still present for $1 < \alpha \lesssim 2$, but it seems to disappear for larger system sizes. For $\alpha > 2$, no size dependence is observed and, according to the bimodal character of the distribution, the variance becomes sensitively larger.

Different information can be extracted by looking at the value of the absolute maximum of the distribution, $\max[P(\ell)]$, shown in Fig. 4(b) (logarithmic scale on the y axis). The first observation is that, in accordance with the variance behavior, the absolute maximum exhibits a strong size dependence for any $\alpha \lesssim 1$. This size dependence is still present at small N for $1 < \alpha \lesssim 2$ to eventually disappear for larger power-law exponents. Then we notice that $\max[P(\ell)]$ shows a nonmonotonic

behavior in α. The absolute minimum occurs not far from the $\alpha_2^\star$ value at which we observed the transition to the area-law regime of the entanglement entropy. Since we do not have any theoretical insight, we do not make any direct connection between the two transitions.

We finally comment that a different scenario emerges for the measurement-only dynamics. In fact, in this case we observe the transition from unimodal to bimodal character at $\bar{\alpha} \sim 1$. As discussed in Sec. IV A, this value corresponds to that of $\alpha_1^\star$, at which we observe the crossover of the entanglement entropy from the volume-law to the subvolume-law phase (c.f. Fig. 2). This result is consistent with the hypothesis that the interplay with the Hamiltonian can generate an intermediate region displaying more complex features. No clear information can be extracted by the analysis of the maxima nor of the moments of the distribution (e.g., the variance).

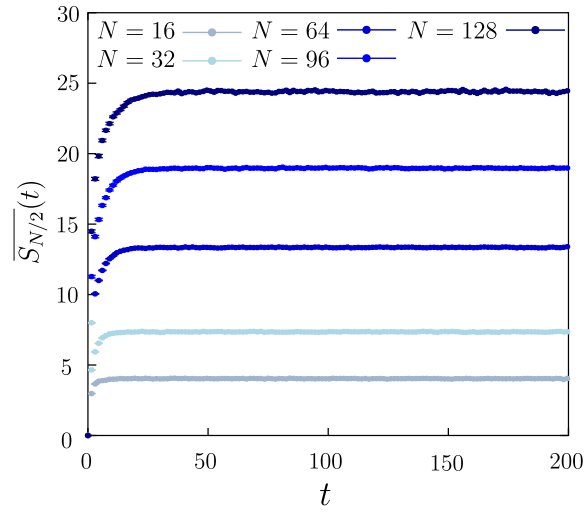

FIG. 5. Behavior of the entanglement entropy in time for different system sizes (color scale), $\gamma = 0.1$, $h = 0.5$, and $\alpha = 2$. After a transient, the entanglement entropy saturates to a value that depends on the system size.

V. CONCLUSIONS

We have studied the dynamics of the entanglement entropy of a fermionic Kitaev chain undergoing a quantum state diffusion evolution, as a result of a continuous measurement process generated by two-point power-law decaying operators. This dynamics preserves the Gaussianity of the state, allowing us to simulate systems up to few hundreds of sites.

First, we focused on the asymptotic entanglement entropy, averaged over the different stochastic measurement processes, both as a function of the system size and of the power-law measurement exponent α. We found three regimes: For $\alpha < \alpha_1^\star$ (with $0.5 \lesssim \alpha_1^\star \lesssim 1$), the entanglement scales linearly with the system size N, that is, as a volume law; on the opposite hand, for $\alpha > \alpha_2^\star$ (with $\alpha_2^\star$ dependent on the parameters of the system). it exhibits a sublogarithmic (probably area-law) scaling.

A similar behavior emerges when considering the measurement-only dynamics. In this case, the transition from volume-law to the nontrivial phase roughly occurs at the same value of $0.5 \lesssim \alpha_1^\star \lesssim 1$ observed for the full Hamiltonian and measurement-induced evolution, suggesting that this transition is an effect of the measurement process only. The other transition point at $\alpha_2^\star$, from the subvolume to the area-law phase, shifts to a smaller power-law exponent. These findings suggest a comparison with the case of one-dimensional long-range Hamiltonians, where also two values of α marking a dynamical transition are present: The investigation of a possible connection between the unitary case and our non-Hermitian dynamics may be the focus of future research.

Second, we considered the expectation probability distribution of the measurement operators. For both the cases of dynamics with and without the Hamiltonian, we have seen that such distribution exhibits a transition from a unimodal to a bimodal behavior, when increasing α above a given threshold $\bar{\alpha}$. However, while for the measurement-only dynamics this transition occurs in correspondence of the $\alpha_1^\star$ at which the entanglement entropy exhibits a transition from volume to subvolume scaling, in the additional presence of the Kitaev Hamiltonian this correspondence disappears. The absolute maximum of the distribution, however, behaves nonmonotonically in α and exhibits a minimum occurring at a power-law exponent that is compatible with the transition from the subvolume to the area-law phase. Nevertheless, this phenomenon is very interesting in itself, being a quantum analog of the bifurcations occurring in classical driven-dissipative dynamical systems. For that reason we dub it a "quantum bifurcation".

In view of the apparently large finite-size effects, to have a confirmation of the stability of the different system behaviors with α, one could look at other quantities as the mutual information or the correlation functions. It would be also tempting to investigate the dependence of these results on the specific unraveling. For example, one can check whether the $\alpha_1^\star$ threshold is robust to the stochastic process chosen to simulate the Lindblad master equation, i.e., whether it is a property of the operator itself, as discussed in [78]. Moreover the effects of long-range measurement operators can be tested in others systems, as quantum circuits [15].

From an experimental perspective, it is important to investigate the connection between the transition of the entanglement entropy and the quantum bifurcation of the distribution.

Before concluding, we mention that a remarkably similar phenomenology has been observed in [93], where a system of monitored two coupled chains of free fermions is considered. In this paper it is shown that it is possible to induce non-Markovian effects on one of the two chains, referred as the system by performing Markovian measurements on the other one, referred as the bath. This non-Markovianity is reflected in the entanglement dynamics that exhibits three different regimes: An area-law scaling, a logarithmic scaling, and a mixed (logarithmic-volume) scaling. Although it could be interesting to investigate the connection between this non-Markovianity and our non-locality, we leave it to future studies.

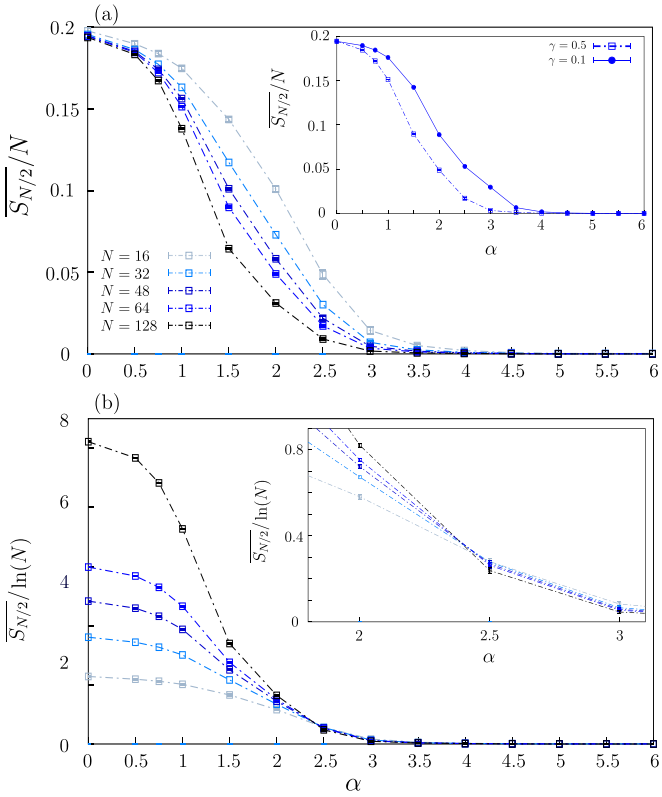

FIG. 6. Average long-time entanglement entropy for the case with Hamiltonian ($J = 1$, $h = 0.5$) and coupling with the environment $\gamma = 0.5$. (a) $S_{N/2}/N$ vs α for different system sizes. The inset shows a comparison of the curves, for fixed size N=64, with $\gamma = 0.5$ and $\gamma = 0.1$. (b) $S_{N/2}/\ln N$ vs α for different system sizes. The inset is a magnification of the same data around $\alpha = 2.5$. Other numerical parameters and initial state as in Fig. 1.

ACKNOWLEDGMENTS

We thank V. Alba, G. Chiriacò, and J. De Nardis for fruitful discussions. We acknowledge financial support from PNRR MUR Project PE0000023-NQSTI. A.R. acknowledges computational resources from MUR, PON "Ricerca e Innovazione 2014-2020", under Grant No. PIR01 00011 - (I.Bi.S.Co.). A.R. thanks the ICTP for the warm hospitality received (under ERC Project 101053159–RAVE) during the preparation of this work. We acknowledge support from the Italian MIUR through PRIN Project No. 2017E44HRF.

APPENDIX A: CONVERGENCE OF THE NUMERICAL RESULTS

All the results have been derived by fixing as integration step $\Delta t = 5 \times 10^{-3}$. This value has been chosen after a convergence check.

The entanglement entropy is defined in Eq. (7), we evaluate its average $S_{N/2}$—defined in Eq. (8)—considering a finite-averaging time T, which has been chosen so that convergence is attained. In Fig. 5 we show the characteristic behavior of $S_{N/2}(t)$ in time for different system sizes (color scale) and $\alpha = 2$. From this figure it is clear that convergence is reached in reasonable times.

The ensemble average is evaluated over $N_{\rm r} \geqslant 48$ trajectories. The inequality means that for small system sizes we can easily average over $N_r = O(10^2)$ trajectories, while for larger N the numerical effort required for the simulations does not allow to go beyond $N_r = 48$.

However, we checked that all the results are consistent inside the error bars $\delta S_{N/2}$, evaluated as

$$\delta S_{N/2} = \frac{1}{\sqrt{N_{\rm r}}} \sqrt{\lim_{T\to\infty} \int_{t^*}^{T} dt' \overline{S^2_{N/2}(t')} - S^2_{N/2}}. \tag{A1}$$

About the numerical implementation, using a FORTRAN code parallelized with Open MPI, in order to get a time trace of the entanglement entropy on a Intel i7 processor with 8 cores of a laptop, for $N = 128$ and $N_r = 48$, one needs more or less three days. Because we needed to do these computations for many points in the parameter space, and also for system sizes larger than $N = 128$, the use of the cluster mentioned in the acknowledgments was more suitable for us.

APPENDIX B: CASE WITH HAMILTONIAN AND $\gamma = 0.5$

Here we provide results for a case similar to the one considered in Fig. 1, with the only difference that now $\gamma = 0.5$. The corresponding numerical data are shown in Fig. 6. Looking at the plot of $S_{N/2}/N$ versus α, we see that the volume law still persists for small α values, up to $0.5 \lesssim \alpha_1^* \lesssim 1$ [Fig. 6(a)]. From the data in inset at fixed size, notice also that, for $\gamma = 0.5$, the entanglement generally drops faster than for $\gamma = 0.1$.

On the other hand, the transition from subvolume law to sublogarithm law occurs for a different value of α_2^* ($\alpha_2^* \sim 2.4$) as we can see from the crossing of the curves of $S_{N/2}/\ln N$ versus α for different sizes N [Fig. 6(b) inset].

[1] M. A. Nielsen and I. L. Chuang, *Quantum Computation and Quantum Information: 10th Anniversary Edition* (Cambridge University Press, Cambridge, 2011).

[2] R. Horodecki, P. Horodecki, M. Horodecki, and K. Horodecki, Quantum entanglement, Rev. Mod. Phys. **81**, 865 (2009).

[3] L. Amico, R. Fazio, A. Osterloh, and V. Vedral, Entanglement in many-body systems, Rev. Mod. Phys. **80**, 517 (2008).

[4] G. Vidal, J. I. Latorre, E. Rico, and A. Kitaev, Entanglement in Quantum Critical Phenomena, Phys. Rev. Lett. **90**, 227902 (2003).

[5] J. I. Latorre, E. Rico, and G. Vidal, Ground state entanglement in quantum spin chains, Quantum Inf. Comput. **4**, 48 (2004).

[6] V. Alba and P. Calabrese, Entanglement and thermodynamics after a quantum quench in integrable systems, Proc. Natl. Acad. Sci. USA **114**, 7947 (2017).

[7] V. Alba and P. Calabrese, Entanglement dynamics after quantum quenches in generic integrable systems, SciPost Phys. **4**, 017 (2018).

[8] R. Singh, J. H. Bardarson, and F. Pollmann, Signatures of the many-body localization transition in the dynamics of

entanglement and bipartite fluctuations, New J. Phys. **18**, 023046 (2016).

[9] A. Russomanno, M. Fava, and R. Fazio, Nonergodic behavior of the clean Bose-Hubbard chain, Phys. Rev. B **102**, 144302 (2020).

[10] D. A. Abanin, E. Altman, I. Bloch, and M. Serbyn, Colloquium: Many-body localization, thermalization, and entanglement, Rev. Mod. Phys. **91**, 021001 (2019).

[11] Y. Li, X. Chen, and M. P. A. Fisher, Quantum Zeno effect and the many-body entanglement transition, Phys. Rev. B **98**, 205136 (2018).

[12] A. Chan, R. M. Nandkishore, M. Pretko, and G. Smith, Unitary-projective entanglement dynamics, Phys. Rev. B **99**, 224307 (2019).

[13] B. Skinner, J. Ruhman, and A. Nahum, Measurement-Induced Phase Transitions in the Dynamics of Entanglement, Phys. Rev. X **9**, 031009 (2019).

[14] M. Szyniszewski, A. Romito, and H. Schomerus, Entanglement transition from variable-strength weak measurements, Phys. Rev. B **100**, 064204 (2019).

[15] A. C. Potter and R. Vasseur, Entanglement dynamics in hybrid quantum circuits, in *Quantum Science and Technology* (Springer International Publishing, New York, 2022), pp. 211–249.

[16] Y. Bao, S. Choi, and E. Altman, Symmetry enriched phases of quantum circuits, Ann. Phys. **435**, 168618 (2021).

[17] A. Nahum and B. Skinner, Entanglement and dynamics of diffusion-annihilation processes with Majorana defects, Phys. Rev. Res. **2**, 023288 (2020).

[18] X. Chen, Y. Li, M. P. A. Fisher, and A. Lucas, Emergent conformal symmetry in nonunitary random dynamics of free fermions, Phys. Rev. Res. **2**, 033017 (2020).

[19] Y. Li, X. Chen, and M. P. A. Fisher, Measurement-driven entanglement transition in hybrid quantum circuits, Phys. Rev. B **100**, 134306 (2019).

[20] C.-M. Jian, Y.-Z. You, R. Vasseur, and A. W. W. Ludwig, Measurement-induced criticality in random quantum circuits, Phys. Rev. B **101**, 104302 (2020).

[21] Y. Li, R. Vasseur, M. P. A. Fisher, and A. W. W. Ludwig, Statistical mechanics model for Clifford random tensor networks and monitored quantum circuits, arXiv:2110.02988.

[22] M. Szyniszewski, A. Romito, and H. Schomerus, Universality of Entanglement Transitions from Stroboscopic to Continuous Measurements, Phys. Rev. Lett. **125**, 210602 (2020).

[23] X. Turkeshi, R. Fazio, and M. Dalmonte, Measurement-induced criticality in $(2+1)$-dimensional hybrid quantum circuits, Phys. Rev. B **102**, 014315 (2020).

[24] O. Lunt, M. Szyniszewski, and A. Pal, Measurement-induced criticality and entanglement clusters: A study of one-dimensional and two-dimensional Clifford circuits, Phys. Rev. B **104**, 155111 (2021).

[25] P. Sierant, M. Schirò, M. Lewenstein, and X. Turkeshi, Measurement-induced phase transitions in $(d+1)$-dimensional stabilizer circuits, Phys. Rev. B **106**, 214316 (2022).

[26] A. Nahum, S. Roy, B. Skinner, and J. Ruhman, Measurement and entanglement phase transitions in all-to-all quantum circuits, on quantum trees, and in Landau-Ginsburg theory, PRX Quantum **2**, 010352 (2021).

[27] A. Zabalo, M. J. Gullans, J. H. Wilson, S. Gopalakrishnan, D. A. Huse, and J. H. Pixley, Critical properties of the measurement-induced transition in random quantum circuits, Phys. Rev. B **101**, 060301(R) (2020).

[28] P. Sierant and X. Turkeshi, Universal Behavior beyond Multifractality of Wave Functions at Measurement-Induced Phase Transitions, Phys. Rev. Lett. **128**, 130605 (2022).

[29] G. Chiriacò, M. Tsitsishvili, D. Poletti, R. Fazio, and M. Dalmonte, Diagrammatic method for many-body non-Markovian dynamics: Memory effects and entanglement transitions Phys. Rev. B **108**, 075151 (2023).

[30] K. Klocke and M. Buchhold, Majorana loop models for measurement-only quantum circuits, arXiv:2305.18559.

[31] X. Cao, A. Tilloy, and A. De Luca, Entanglement in a fermion chain under continuous monitoring, SciPost Phys. **7**, 024 (2019).

[32] M. Buchhold, Y. Minoguchi, A. Altland, and S. Diehl, Effective Theory for the Measurement-Induced Phase Transition of Dirac Fermions, Phys. Rev. X **11**, 041004 (2021).

[33] C.-M. Jian, B. Bauer, A. Keselman, and A. W. W. Ludwig, Criticality and entanglement in nonunitary quantum circuits and tensor networks of noninteracting fermions, Phys. Rev. B **106**, 134206 (2022).

[34] M. Coppola, E. Tirrito, D. Karevski, and M. Collura, Growth of entanglement entropy under local projective measurements, Phys. Rev. B **105**, 094303 (2022).

[35] M. Fava, L. Piroli, T. Swann, D. Bernard, and A. Nahum, Nonlinear sigma models for monitored dynamics of free fermions, arXiv:2302.12820.

[36] I. Poboiko, P. Pöpperl, I. V. Gornyi, and A. D. Mirlin, Theory of free fermions under random projective measurements arXiv:2304.03138.

[37] C.-M. Jian, H. Shapourian, B. Bauer, and A. W. W. Ludwig, Measurement-induced entanglement transitions in quantum circuits of non-interacting fermions: Born-rule versus forced measurements, arXiv:2302.09094.

[38] J. Merritt and L. Fidkowski, Entanglement transitions with free fermions, Phys. Rev. B **107**, 064303 (2023).

[39] O. Alberton, M. Buchhold, and S. Diehl, Entanglement Transition in a Monitored Free-Fermion Chain: From Extended Criticality to Area Law, Phys. Rev. Lett. **126**, 170602 (2021).

[40] X. Turkeshi, A. Biella, R. Fazio, M. Dalmonte, and M. Schirò, Measurement-induced entanglement transitions in the quantum Ising chain: From infinite to zero clicks, Phys. Rev. B **103**, 224210 (2021).

[41] M. Szyniszewski, O. Lunt, and A. Pal, Disordered monitored free fermions, arXiv:2211.02534.

[42] X. Turkeshi, M. Dalmonte, R. Fazio, and M. Schirò, Entanglement transitions from stochastic resetting of non-Hermitian quasiparticles, Phys. Rev. B **105**, L241114 (2022).

[43] G. Piccitto, A. Russomanno, and D. Rossini, Entanglement transitions in the quantum Ising chain: A comparison between different unravelings of the same Lindbladian, Phys. Rev. B **105**, 064305 (2022).

[44] G. Piccitto, A. Russomanno, and D. Rossini, Erratum: Entanglement transitions in the quantum Ising chain: A comparison between different unravelings of the same Lindbladian, Phys. Rev. B **106**, 219901(E) (2022).

[45] E. Tirrito, A. Santini, R. Fazio, and M. Collura, Full counting statistics as probe of measurement-induced transitions in the quantum Ising chain, SciPost Phys. **15**, 096 (2023)

[46] A. Paviglianiti and A. Silva, Multipartite entanglement in the measurement-induced phase transition of the quantum Ising chain, arXiv:2302.06477.

[47] O. Lunt and A. Pal, Measurement-induced entanglement transitions in many-body localized systems, Phys. Rev. Res. **2**, 043072 (2020).

[48] D. Rossini and E. Vicari, Measurement-induced dynamics of many-body systems at quantum criticality, Phys. Rev. B **102**, 035119 (2020).

[49] Q. Tang and W. Zhu, Measurement-induced phase transition: A case study in the nonintegrable model by density-matrix renormalization group calculations, Phys. Rev. Res. **2**, 013022 (2020).

[50] Y. Fuji and Y. Ashida, Measurement-induced quantum criticality under continuous monitoring, Phys. Rev. B **102**, 054302 (2020).

[51] P. Sierant, G. Chiriacó, F. M. Surace, S. Sharma, X. Turkeshi, M. Dalmonte, R. Fazio, and G. Pagano, Dissipative Floquet dynamics: From steady state to measurement induced criticality in trapped-ion chains, Quantum **6**, 638 (2022).

[52] E. V. H. Doggen, Y. Gefen, I. V. Gornyi, A. D. Mirlin, and D. G. Polyakov, Generalized quantum measurements with matrix product states: Entanglement phase transition and clusterization, Phys. Rev. Res. **4**, 023146 (2022).

[53] A. Altland, M. Buchhold, S. Diehl, and T. Micklitz, Dynamics of measured many-body quantum chaotic systems, Phys. Rev. Res. **4**, L022066 (2022).

[54] M. J. Gullans and D. A. Huse, Scalable Probes of Measurement-Induced Criticality, Phys. Rev. Lett. **125**, 070606 (2020).

[55] M. J. Gullans and D. A. Huse, Dynamical Purification Phase Transition Induced by Quantum Measurements, Phys. Rev. X **10**, 041020 (2020).

[56] H. Lóio, A. De Luca, J. De Nardis, and X. Turkeshi, Purification timescales in monitored fermions Phys. Rev. B **108**, L020306 (2023).

[57] S. Choi, Y. Bao, X.-L. Qi, and E. Altman, Quantum Error Correction in Scrambling Dynamics and Measurement-Induced Phase Transition, Phys. Rev. Lett. **125**, 030505 (2020).

[58] Y. Bao, S. Choi, and E. Altman, Theory of the phase transition in random unitary circuits with measurements, Phys. Rev. B **101**, 104301 (2020).

[59] L. Fidkowski, J. Haah, and M. B. Hastings, How dynamical quantum memories forget, Quantum **5**, 382 (2021).

[60] Y. Bao, M. Block, and E. Altman, Finite time teleportation phase transition in random quantum circuits, arXiv:2110.06963.

[61] F. Barratt, U. Agrawal, A. C. Potter, S. Gopalakrishnan, and R. Vasseur, Transitions in the Learnability of Global Charges from Local Measurements, Phys. Rev. Lett. **129**, 200602 (2022).

[62] H. Dehghani, A. Lavasani, M. Hafezi, and M. J. Gullans, Neural-network decoders for measurement induced phase transitions, Nat. Commun. **14**, 2918 (2023).

[63] S. P. Kelly, U. Poschinger, F. Schmidt-Kaler, M. P. A. Fisher, and J. Marino, Coherence requirements for quantum communication from hybrid circuit dynamics, arXiv:2210.11547.

[64] M. Ippoliti, M. J. Gullans, S. Gopalakrishnan, D. A. Huse, and V. Khemani, Entanglement Phase Transitions in Measurement-Only Dynamics, Phys. Rev. X **11**, 011030 (2021).

[65] A. Sriram, T. Rakovszky, V. Khemani, and M. Ippoliti, Topology, criticality, and dynamically generated qubits in a stochastic measurement-only Kitaev model, arXiv:2207.07096.

[66] N. Lang and H. P. Büchler, Entanglement transition in the projective transverse field Ising model, Phys. Rev. B **102**, 094204 (2020).

[67] T. Minato, K. Sugimoto, T. Kuwahara, and K. Saito, Fate of Measurement-Induced Phase Transition in Long-Range Interactions, Phys. Rev. Lett. **128**, 010603 (2022).

[68] C. Zerba and A. Silva, Measurement phase transitions in the no-click limit as quantum phase transitions of a non-Hermitean vacuum, SciPost Phys. Core **6**, 051 (2023).

[69] T. Müller, S. Diehl, and M. Buchhold, Measurement-Induced Dark State Phase Transitions in Long-Ranged Fermion Systems, Phys. Rev. Lett. **128**, 010605 (2022).

[70] M. Block, Y. Bao, S. Choi, E. Altman, and N. Y. Yao, Measurement-Induced Transition in Long-Range Interacting Quantum Circuits, Phys. Rev. Lett. **128**, 010604 (2022).

[71] S. Sharma, X. Turkeshi, R. Fazio, and M. Dalmonte, Measurement-induced criticality in extended and long-range unitary circuits, SciPost Phys. Core **5**, 023 (2022).

[72] G. Piccitto, A. Russomanno, and D. Rossini, Entanglement dynamics with string measurement operators, arXiv:2303.07102.

[73] N. Gisin and I. C. Percival, The quantum-state diffusion model applied to open systems, J. Phys. A: Math. Theor. **25**, 5677 (1992).

[74] K. Jacobs, *Quantum Measurement Theory and its Applications* (Cambridge University Press, Cambridge, 2014).

[75] K. Seetharam, A. Lerose, R. Fazio, and J. Marino, Correlation engineering via nonlocal dissipation, Phys. Rev. Res. **4**, 013089 (2022).

[76] K. Seetharam, A. Lerose, R. Fazio, and J. Marino, Dynamical scaling of correlations generated by short- and long-range dissipation, Phys. Rev. B **105**, 184305 (2022).

[77] J. Marino, Universality Class of Ising Critical States with Long-Range Losses, Phys. Rev. Lett. **129**, 050603 (2022).

[78] G. Passarelli, P. Lucignano, R. Fazio, and A. Russomanno, Dissipative time crystals with long-range Lindbladians, Phys. Rev. B **106**, 224308 (2022).

[79] G. Passarelli, X. Turkeshi, A. Russomanno, P. Lucignano, M. Schiró, and R. Fazio, Post-selection-free measurement-induced phase transition in driven atomic gases with collective decay, arXiv:2306.00841.

[80] A. Campa, T. Dauxois, D. Fanelli, and S. Ruffo, *Physics of Long-Range Interacting Systems* (Oxford University Press, Oxford, 2014).

[81] B. Žunkovič, M. Heyl, M. Knap, and A. Silva, Dynamical Quantum Phase Transitions in Spin Chains with Long-Range Interactions: Merging Different Concepts of Nonequilibrium Criticality, Phys. Rev. Lett. **120**, 130601 (2018).

[82] S. Strogatz, *Nonlinear Dynamics and Chaos: With Applications to Physics, Biology, Chemistry, and Engineering*, 2nd ed. (Taylor & Francis, London, 2015).

[83] M. Cross and H. Greenside, *Pattern Formation and Dynamics in Nonequilibrium Systems* (Cambridge University Press, Cambridge, 2009).

[84] A. Y. Kitaev, Unpaired Majorana fermions in quantum wires, Phys. Usp. **44**, 131 (2001).

[85] S. Sachdev, *Quantum Phase Transitions* (Cambridge University Press, Cambridge, 2011).

[86] P. Pfeuty, The one-dimensional Ising model with a transverse field, Ann. Phys. **57**, 79 (1970).

[87] M. Kac, G. Uhlenbeck, and P. Hemmer, On the van der Waals theory of the vapor-liquid equilibrium. I. Discussion of a one-dimensional model, J. Math. Phys. **4**, 216 (1963).

[88] G. B. Mbeng, A. Russomanno, and G. E. Santoro, The quantum Ising chain for beginners, arXiv:2009.09208.

[89] T. Zanca and G. E. Santoro, Quantum annealing speedup over simulated annealing on random Ising chains, Phys. Rev. B **93**, 224431 (2016).

[90] Deriving Eq. (20) with respect to t', we get

$$\left[\frac{d}{dt'}\mathbf{U}^{\dagger}(t')\right]\mathbf{Z}(t') + \mathbf{U}^{\dagger}(t')\frac{d}{dt'}\mathbf{Z}(t') = -\frac{d}{dt'}\mathbf{V}^{\dagger}(t').$$

Substituting in it Eqs. (16) and (21), we get an identity.

[91] B. Ladewig, S. Diehl, and M. Buchhold, Monitored open fermion dynamics: Exploring the interplay of measurement, decoherence, and free Hamiltonian evolution, Phys. Rev. Res. **4**, 033001 (2022).

[92] X. Turkeshi, L. Piroli, and M. Schirò, Density and current statistics in boundary-driven monitored fermionic chains, arXiv:2306.09893.

[93] M. Tsitsishvili, D. Poletti, M. Dalmonte, and G. Chiriacò, Measurement induced transitions in non-Markovian free fermion ladders, arXiv:2307.06624.